Cold Nuclear Matter Effects on J/ψ Production

R. Vogt

Lawrence Livermore National Laboratory, Livermore, CA 94551, USA
Physics and Astronomy Department, UC Davis, Davis, CA 95616, USA

based on:
RV, arXiv:2101.02858, Phys. Rev. C 103, 035204 (2021)
RV, arXiv:2207.04347, Phys. Rev. C 106, 025201 (2022)
RV, in progress

Figure 1: This work was performed under the auspices of the U.S. Department of Energy by Lawrence Livermore National Laboratory under Contract DE-AC52-07NA27344 and the LLNL-LDRD Program under Project No. 21-LW-034.

Charmonium Production in Color Evaporation Model

The CEM at NLO is employed for the perturbative production cross section:

$$\sigma_{\rm CEM}(pp) = F_C \sum_{i,j} \int_{4m^2}^{4m_H^2} ds \int dx_1\, dx_2\ F_i^p(x_1, \mu_F^2, k_{T_1})\ F_j^p(x_2, \mu_F^2, k_{T_2})\ \hat{\sigma}_{ij}(\hat{s}, \mu_F^2, \mu_R^2)$$

Parton densities factorized into longitudinal (CT10) and a k_T-dependent component to implement k_T broadening a la low p_T resummation

$$F^p(x, \mu_F^2, k_T) = f^p(x, \mu_F^2) G_p(k_T) \quad G_p(k_T) \ = \ \frac{1}{\pi \langle k_T^2 \rangle_p} \exp(-k_T^2/\langle k_T^2 \rangle_p)$$

$$\langle k_T^2 \rangle_p = \left[1 + \frac{1}{n} \ln \left(\frac{\sqrt{s_{NN}}(\mathrm{GeV})}{20\,\mathrm{GeV}} \right) \right] \ \mathrm{GeV}^2$$

$\langle k_T^2 \rangle_p$ **broadening assumed energy dependent,** $n = 12$ **from** J/ψ **data**

Uncertainty bands defined by $(m, \mu_F/m_T, \mu_R/m_T) = (1.27 \pm 0.09\,\mathrm{GeV}, 2.1^{+2.55}_{-0.85}, 1.6^{+0.11}_{-0.12})$**;** μ_F**, factorization scale, and** μ_R**, renormalization scale, defined relative to pair** m_T**:** $\mu_{F,R} \propto m_T = \sqrt{m^2 + p_T^2}$ **where** $p_T^2 = 0.5(p_{T_Q}^2 + p_{T_{\overline{Q}}}^2)$

Scale uncertainties set by $\{(\mu_F/m_T, \mu_F/m_T)\} = \{(C,C)$**,** (H,H)**,** (L,L)**,** (C,L)**,** (L,C)**,** (C,H)**,** $(H,C)\}$ **(Mass uncertainties dominate.)**

$$\frac{d\sigma_{\rm max}}{dX} \ = \ \frac{d\sigma_{\rm cent}}{dX} + \sqrt{\left(\frac{d\sigma_{\mu,{\rm max}}}{dX} - \frac{d\sigma_{\rm cent}}{dX}\right)^2 + \left(\frac{d\sigma_{m,{\rm max}}}{dX} - \frac{d\sigma_{\rm cent}}{dX}\right)^2}$$

$$\frac{d\sigma_{\rm min}}{dX} \ = \ \frac{d\sigma_{\rm cent}}{dX} - \sqrt{\left(\frac{d\sigma_{\mu,{\rm min}}}{dX} - \frac{d\sigma_{\rm cent}}{dX}\right)^2 + \left(\frac{d\sigma_{m,{\rm min}}}{dX} - \frac{d\sigma_{\rm cent}}{dX}\right)^2}$$

Cold Matter Effects on Perturbative Cross Section

Production cross section in a pA collision is

$$\sigma_{pA} = \sigma_{\rm CEM}(pA) = S_A^{\rm abs} F_C \sum_{i,j} \int_{4m^2}^{4m_H^2} ds \int dx_1\, dx_2 \;\; F_i^p(x_1,\mu_F^2,k_T) \;\; F_j^A(x_2,\mu_F^2,k_T) \;\; \hat\sigma_{ij}(\hat s,\mu_F^2,\mu_R^2)$$

Survival probability for absorption of a (proto)charmonium state in nuclear matter:

$$\begin{aligned}\sigma_{pA} = \sigma_{pN} S_A^{\rm abs} &= \sigma_{pN} \int d^2b \int_{-\infty}^{\infty} dz\, \rho_A(b,z) S^{\rm abs}(b) \\ &= \sigma_{pN} \int d^2b \int_{-\infty}^{\infty} dz\, \rho_A(b,z) \exp\left\{ - \int_z^{\infty} dz' \rho_A(b,z') \sigma_{\rm abs}(z'-z) \right\}\end{aligned}$$

The absorption cross section is assumed constant. Prior fixed-target experiments extracted an effective absorption cross section from A^α analysis with $\alpha = 1 - 9\sigma_{\rm abs}/(16\pi r_0^2)$ assuming no other nuclear effects

Nuclear parton densities

$$\begin{aligned}F_j^A(x_2,\mu_F^2,k_T) &= R_j(x_2,\mu_F^2,A) f_j(x_2,\mu_F^2) G_A(k_T) \\ F_i^p(x_1,\mu_F^2,k_T) &= f_i(x_1,\mu_F^2) G_p(k_T)\end{aligned}$$

$G_A(k_T)$ **includes increased broadening in the nuclear target** ($A > 2$)

k_T Broadening in Nuclei

k_T broadening in nuclei may be enhanced through multiple scattering in the target; to implement enhanced broadening, a larger value of $\langle k_T^2 \rangle$ is used for nuclear targets

$$\langle k_T^2 \rangle_A = \langle k_T^2 \rangle_p + \delta k_T^2$$

δk_T^2 gives strength of broadening

$$\delta k_T^2 = (\langle \nu \rangle - 1)\Delta^2(\mu)$$

The broadening strength depends on the interaction scale:

$$\Delta^2(\mu) = 0.225 \frac{\ln^2(\mu/\mathrm{GeV})}{1+\ln(\mu/\mathrm{GeV})} \mathrm{GeV}^2 \qquad \mu = 2m_c$$

Strength also depends on number of scatterings proton undergoes passing through nuclear target, $\langle \nu \rangle - 1$

$$\langle \nu \rangle = \sigma_{pp}^{\mathrm{in}} \frac{\int d^2b T_A^2(b)}{\int d^2b T_A(b)} = \frac{3}{2}\rho_0 R_A \sigma_{pp}^{\mathrm{in}}$$

T_A is the nuclear profile function, here $\rho_0 = 0.16/\mathbf{fm}^3$, $R_A = 1.2A^{1/3}$, and the inelastic $p+p$ cross section is $\sigma_{pp}^{\mathrm{in}} \sim 30$ mb for the energies considered here

Nuclear Modification of the Parton Densities

EPPS16 nuclear parton density modifications differentiate between u and d valence quarks and all sea quarks; 20 parameters give 40 error sets + 1 central set

EPPS21 has 24 parameters but somewhat smaller uncertainties

Uncertainties are determined by calculating cross section for each A with all error sets, adding differences around central set for each parameter in quadrature

Lower energies probe higher x, for $0 < y < 1$, the momentum fraction in the nucleus is in the antishadowing and EMC regions (see right-hand plot)

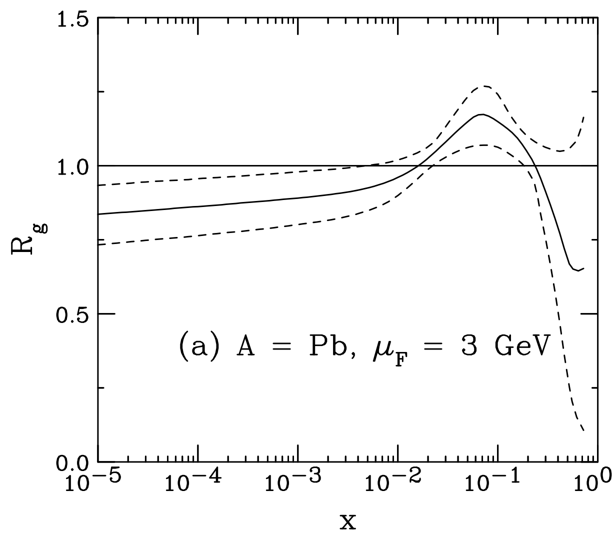

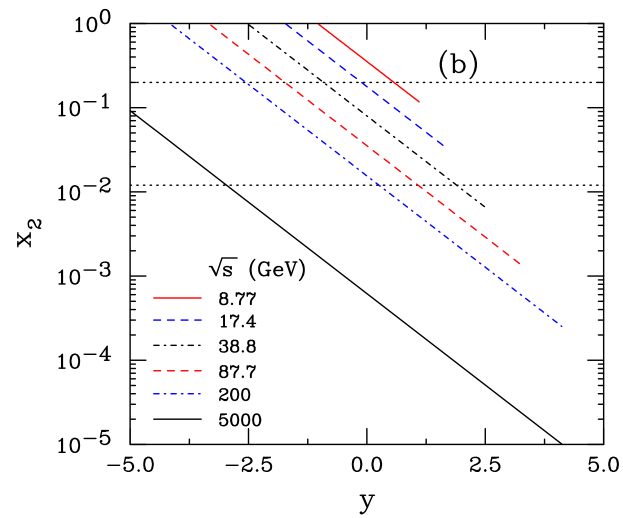

Figure 2: (Left) The EPPS16 ratio for a lead nucleus, with uncertainties, is shown at the scale of the J/ψ mass for gluons as a function of momentum fraction x. The central set is denoted by the solid curves while the dashed curves give the upper and lower limits of the uncertainty bands. (Right) The x_2 range as a function of rapidity for six values of $\sqrt{s_{NN}}$ covering a range of energies using nuclear targets: 8.77 (solid red), 17.4 (dashed blue), 38.8 (dot-dashed black), 87.7 (dashed red), 200 (dot-dashed blue) and 5000 (solid black) GeV. The upper and lower dotted lines at $x_2 = 0.012$ and 0.2 represent the lower and upper limits of the antishadowing region for $\mu_F = 3$ GeV.

Energy Dependence of $\sigma_{\rm abs}^{J/\psi}$

At midrapidity, systematic decrease of $\sigma_{\rm abs}^{J/\psi}$ with $\sqrt{s_{NN}}$, independent of shadowing although $\sigma_{\rm abs}^{J/\psi}$ extracted from data can dependn on shadowing parameterization and x region

$\sigma_{\rm abs}^{J/\psi}(y_{\rm cms} = 0)$ at 158 GeV is significantly larger than that measured at 450 GeV

Calculations confirmed by NA60 pA measurements at 158 GeV showing stronger absorption with L than at 400 GeV, suggesting $\sigma_{\rm abs}^{J/\psi} = 9$ mb at $\sqrt{s_{NN}} = 15.4$ GeV, 5 mb at $\sqrt{s_{NN}} = 38.8$ GeV

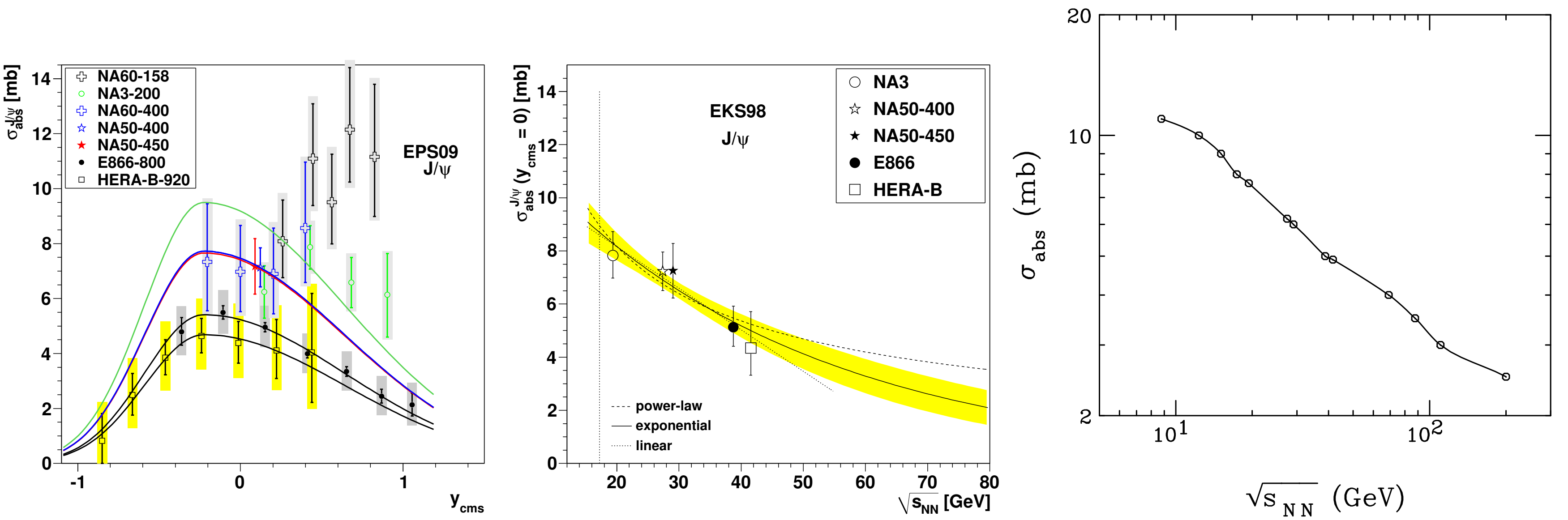

Figure 3: Left: Dependence of $\sigma_{\rm abs}^{J/\psi}$ on $y_{\rm cms}$ for all available data sets including EPS09 shadowing. The shape of the curves is fixed by the E866 and HERA-B data. [Lourenço, RV, Wöhri] Middle: The extracted energy dependence of $\sigma_{\rm abs}^{J/\psi}$ at midrapidity for power law (dashed), exponential (solid) and linear (dotted) approximations to $\sigma_{\rm abs}^{J/\psi}(y = 0, \sqrt{s_{NN}})$ using the EKS98 shadowing parameterization with the CTEQ61L parton densities. The band around the exponential curve indicates the uncertainty in the extracted cross sections at $x_F \sim 0$ from NA3, NA50 at 400 and 450 GeV, E866 and HERA-B. The vertical dotted line indicates the energy of the Pb+Pb and In+In collisions at the CERN SPS. [Lourenço, RV, Wöhri] Right: The value of $\sigma_{\rm abs}$ as a function of $\sqrt{s_{NN}}$. The points show the energies used here. The line is meant to guide the eye.

Intrinsic Charm

Probability distribution of five-particle Fock state of the proton:

$$dP_{\mathrm{ic}\,5} = P^0_{\mathrm{ic}\,5} N_5 \int dx_1 \cdots dx_5 \int dk_{x\,1} \cdots dk_{x\,5} \int dk_{y\,1} \cdots dk_{y\,5} \frac{\delta(1 - \sum_{i=1}^5 x_i)\delta(\sum_{i=1}^5 k_{x\,i})\delta(\sum_{i=1}^5 k_{y\,i})}{(m_p^2 - \sum_{i=1}^5 (\widehat{m}_i^2/x_i))^2}$$

$i = 1, 2, 3$ **are** u, u, d **light quarks, 4 and 5 are** c **and** $\overline{c}$**,** N_t **normalizes the probability to unity and** P^0_{ic} **scales the normalized probability to the assumed intrinsic charm content: 0.1%, 0.31% and 1% are used to represent the range of probabilities assumed previously**

The IC cross section is determined from soft interaction scale breaking coherence of the Fock state, $\mu^2 = 0.1$ **GeV**^{2}

$$\sigma_{\mathrm{ic}}(pp) = P_{\mathrm{ic}\,5} \sigma^{\mathrm{in}}_{pN} \frac{\mu^2}{4\widehat{m}_c^2}$$

The J/ψ **cross section from intrinsic charm is then obtained by multiplying by the normalization factor for the CEM to the** J/ψ

$$\sigma^{J/\psi}_{\mathrm{ic}}(pp) = F_C \sigma_{\mathrm{ic}}(pp)$$

The A **dependence is**

$$\sigma^{J/\psi}_{\mathrm{ic}}(pA) = \sigma^{J/\psi}_{\mathrm{ic}}(pp)\, A^\beta$$

where $\beta = 0.71$ **for a proton beam on a nuclear target, as determined by NA3**

LHCb: Evidence of Intrinsic Charm in $Z + c$-Jet Events

$Z+c$-jet ratio to Z+all-jet events at $\sqrt{s} = 13$ TeV is more consistent with calculations including intrinsic charm at high $y(Z)$, up to 1% intrinsic charm content

Differences between calculations without intrinsic charm (no IC) and intrinsic charm allowed calculations, either with NNPDF 3.0 including IC or CT14 with a 1% IC content, grows larger with increasing $y(Z)$

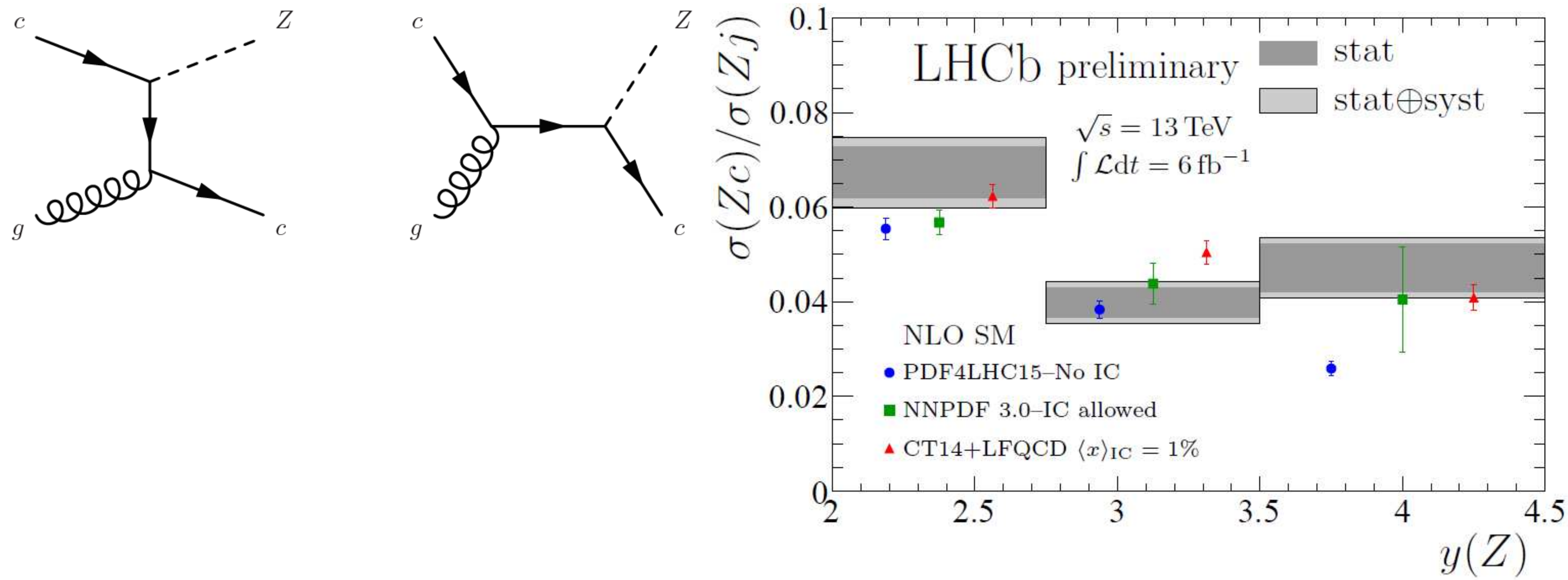

Figure 4: (Left) Leading order diagrams producing $Z + c$-jet events. (Right) Ratio of $Z + c$-jets to Z+all-jet events from LHCb. Images from https://lhcb-public.web.cern.ch/Welcome.html#IC, 27 July 2021.

Intrinsic Charm x_F and y Distributions

Peak of the J/ψ x_F distribution is forward, independent of $\sqrt{s}$

After transforming x_F to rapidity, the distributions depend on $\sqrt{s_{NN}}$: $x_F = (2m_T/\sqrt{s_{NN}})\sinh y$

As $\sqrt{s_{NN}}$ increases, the intrinsic charm rapidity distribution is boosted away from midrapidity until, at $\sqrt{s_{NN}} = 7$ TeV, it is inaccessible to most forward detectors

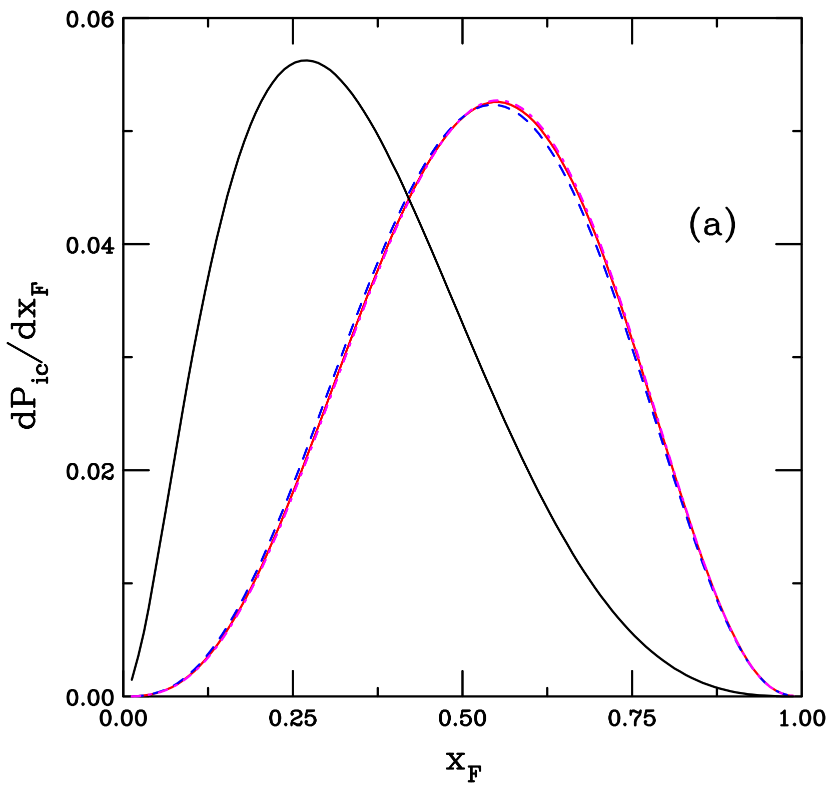

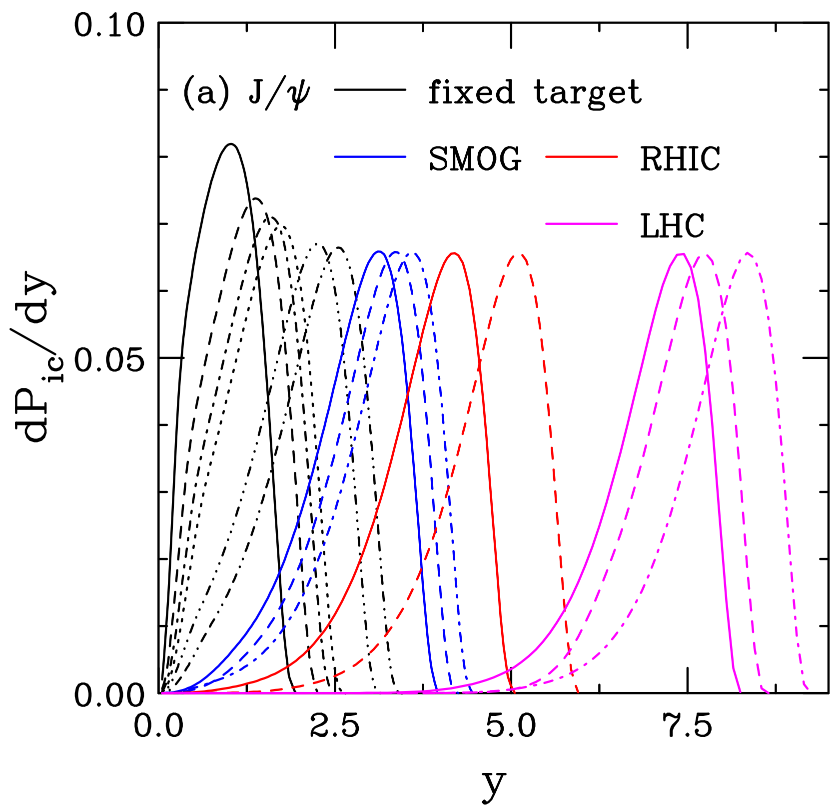

Figure 5: The probability distributions for J/ψ production from a five-particle proton Fock state as a function of x_F (left) and y (right). The results on the left-hand side are shown for different values of the k_T range for the light and charm quarks. The red curve employs the default values, $k_q^{\rm max} = 0.2$ GeV and $k_c^{\rm max} = 1.0$ GeV while the blue dashed curve increases $k_q^{\rm max}$ and $k_c^{\rm max}$ by a factor of two and the dot-dashed magenta curve employs half the values of $k_q^{\rm max}$ and $k_c^{\rm max}$. The solid black curve shows the x and p_T distributions for a single charm quark from the state. On the right-hand side, the results are shown for different values of $\sqrt{s_{NN}}$ from $\sqrt{s_{NN}} = 8.8$ GeV to 13 TeV.

y Dependence of IC p_T Distributions

The intrinsic charm p_T distribution depends slightly on the range of k_T integrations but more strongly on rapidity range

The green curve (right) is integrated over all y while a cut on the p_T distribution for $0 < y < 1$ reduces contribution to low p_T region

At higher energies there is no contribution from intrinsic charm at low p_T and midrapidity

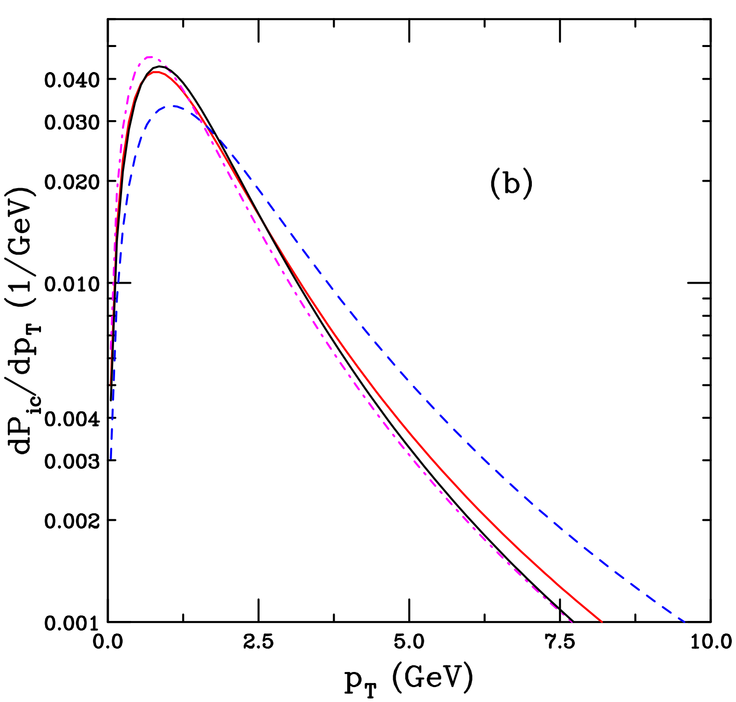

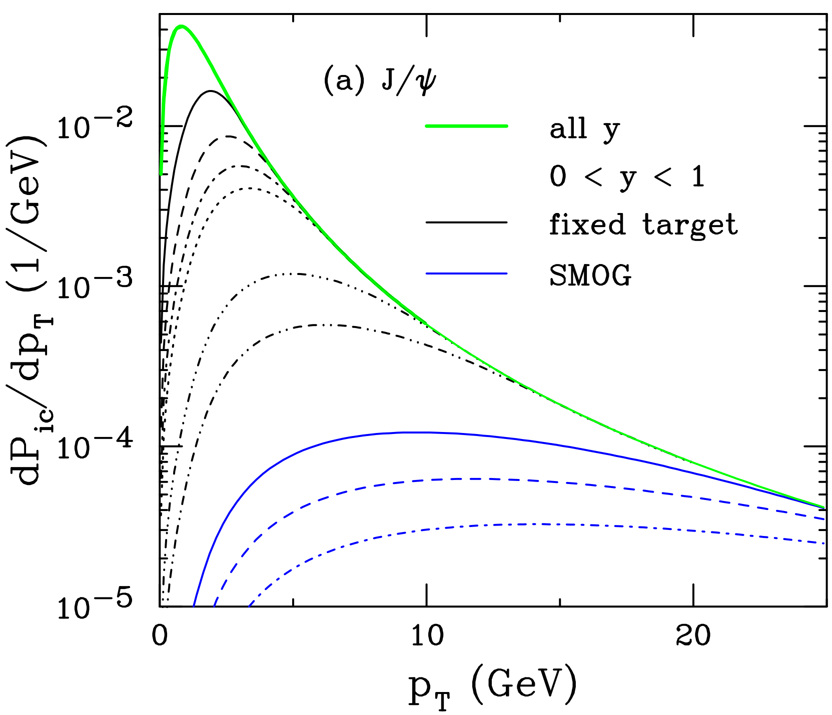

Figure 6: (Left) The probability distributions for J/ψ production from a five-particle proton Fock state as a function of p_T, over all rapidity. The results are shown for different values of the k_T range for the light and charm quarks. The red curve employs the default values, $k_q^{\rm max} = 0.2$ GeV and $k_c^{\rm max} = 1.0$ GeV while the blue dashed curve increases $k_q^{\rm max}$ and $k_c^{\rm max}$ by a factor of two and the dot-dashed magenta curve employs half the values of $k_q^{\rm max}$ and $k_c^{\rm max}$. The solid black curve shows the x and p_T distributions for a single charm quark from the state. (Right) The J/ψ p_T distribution in the range $0 < y < 1$ for energies from $\sqrt{s_{NN}} = 8.8$ GeV to 110 GeV.

Model Calculation

Focus in this talk is on J/ψ but the same calculational structure holds for $\overline{D}$ mesons

The $p+p$ and $p+\mathrm{Pb}$ distributions are shown at the same energy as a function of rapidity and transverse momentum; the nuclear suppression factor, $R_{p\mathrm{Pb}}$ is also shown

The nuclear suppression factor includes both the perturbative cross section and production by intrinsic charm:

$$\begin{aligned} \sigma_{pA} &= \sigma_{\mathrm{CEM}}(pA) + \sigma_{\mathrm{ic}}^{J/\psi}(pA) \\ \sigma_{pp} &= \sigma_{\mathrm{CEM}}(pp) + \sigma_{\mathrm{ic}}^{J/\psi}(pp) \end{aligned}$$

σ_{CEM} is the production cross section computed at NLO in the color evaporation model for $p+p$ and $p+A$ interactions

$\sigma_{\mathrm{ic}}^{J/\psi}$ is intrinsic charm production cross section including the probability for an intrinsic charm contribution to the proton wavefunction

$p+p$ and $p+\mathrm{Pb}$ distributions as a function of y and p_T

Here the p_T distribution is taken in the range $0 < |y| < 1$ for $p_{\rm lab} = 40$ and 800 GeV and $1.1 < |y| < 2.2$ for $\sqrt{s_{NN}} = 200$ GeV

An enhanced k_T broadening is assumed for $p+\mathrm{Pb}$ collisions

The A dependence of intrinsic charm suppresses its contribution in the lead nucleus

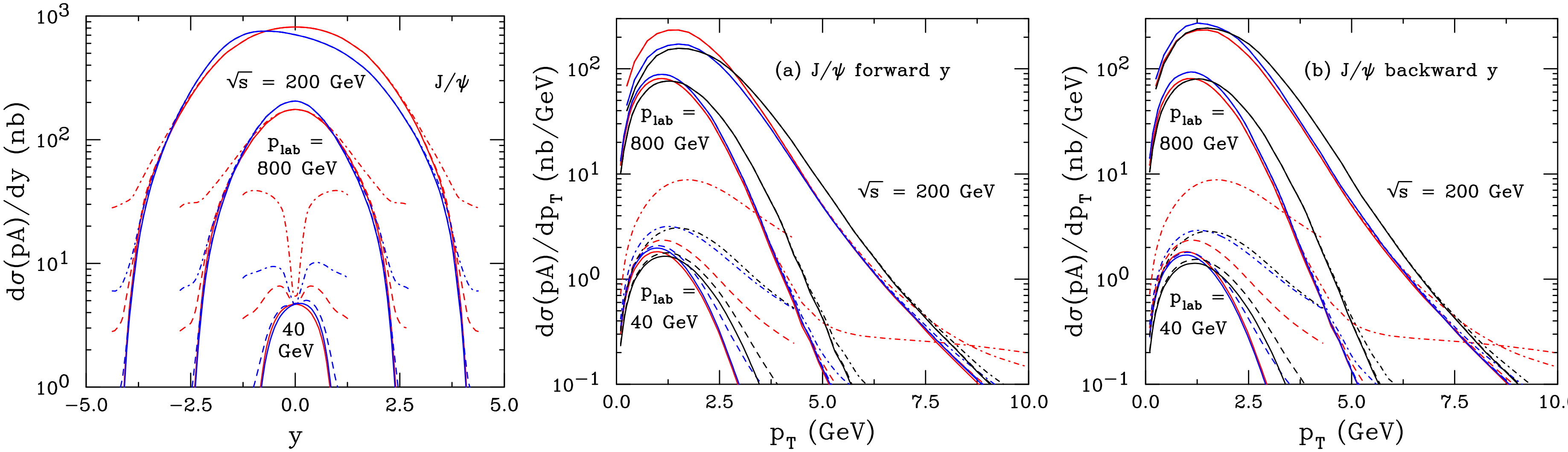

Figure 7: The J/ψ distributions at $p+p$ and $p+\mathrm{Pb}$ (per nucleon) at $p_{\rm lab} = 40$ and 800 GeV and $\sqrt{s} = 200$ GeV as a function of rapidity (left) and forward (middle, a) and backward (right, b) rapidity. The red curves show the results for $p+p$ collisions while the blue and black curves show the $p+\mathrm{Pb}$ distributions without and with an enhanced intrinsic k_T kick respectively. (The rapidity distributions are independent of the kick.) Three curves are shown in each case: no intrinsic charm (pQCD only, solid); $P^0_{\rm ic\,5} = 0.1\%$ (dashed); and $P^0_{\rm ic\,5} = 1\%$ (dot-dashed). No J/ψ absorption by nucleons is considered in the $p+\mathrm{Pb}$ calculation.

Summary of Previous Fixed-Target J/ψ Data

NA60 $p_{\rm lab} = 158$ **and 400 GeV, covering** $0.05 < x_F < 0.4$ **and** $-0.075 < x_F < 0.125$ **respectively, were taken on Be, Al, Cu, In, W, Pb, and U targets (PLB 706, 263 (2012))**

NA3 $p_{\rm lab} = 200$ **GeV,** $x_F > 0$**, taken on a Pt target (Z. Phys. C 20, 101 (1983))**

NA50 $p_{\rm lab} = 450$ **GeV, midrapidity (**$-0.1 < x_F < 0.1$**), used Be, Al, Cu, Ag, W and Pb targets (EPJ C 33, 31 (2004))**

E866 $p_{\rm lab} = 800$ **GeV,** $-0.09 < x_F < 0.95$**, used Be, Fe, and W targets (PRL 84, 3256 (2000))**

HERA-B $p_{\rm lab} = 920$ **GeV,** $-0.34 < x_F < 0.14$**, used C, Ti and W targets (EPJ C 60, 525 (2009))**

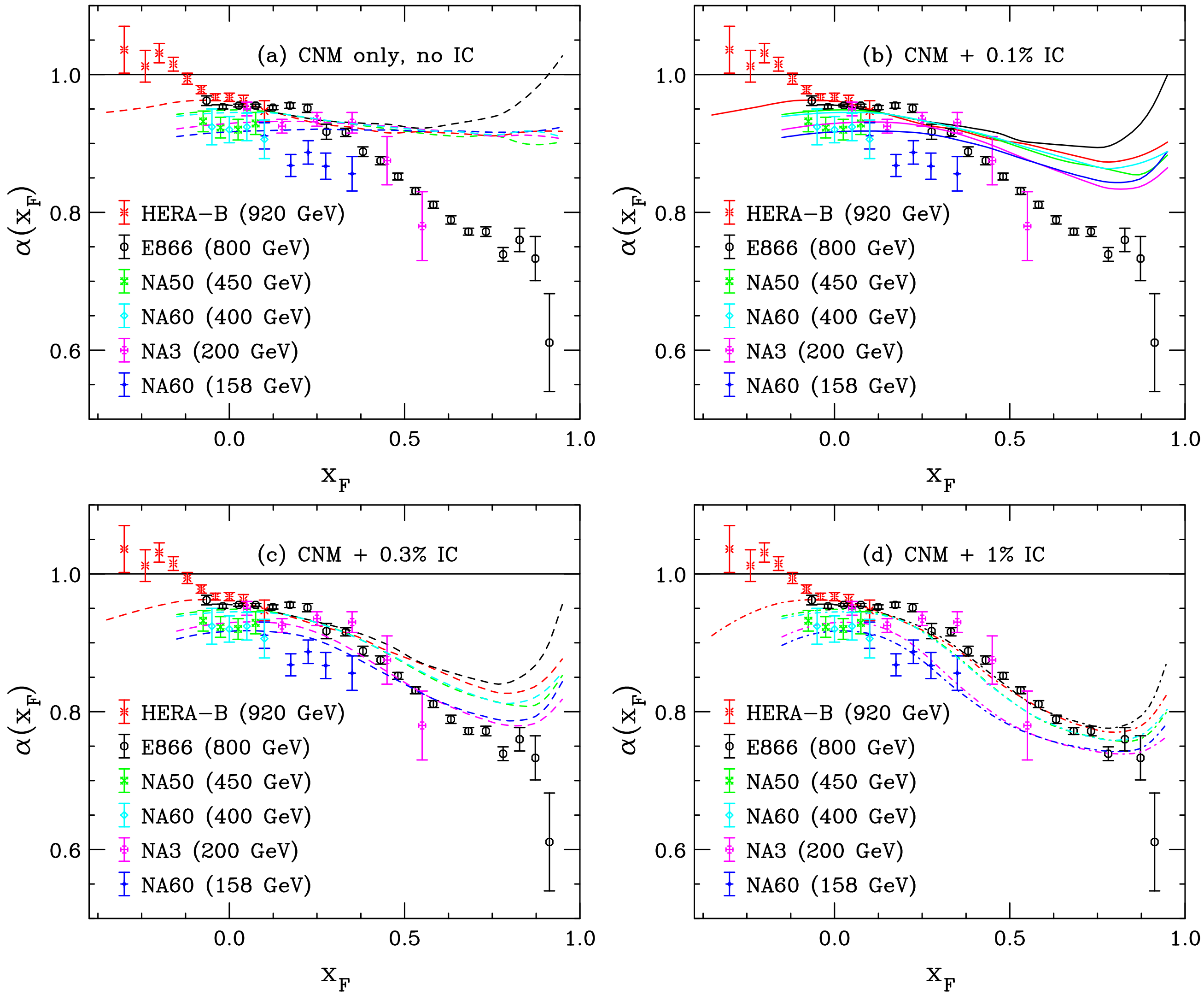

Figure 8: The J/ψ $\alpha(x_F)$ at: NA60 ($p_{\rm lab} = 158$ GeV), NA3 ($p_{\rm lab} = 200$ GeV), NA60 ($p_{\rm lab} = 400$ GeV), NA50 ($p_{\rm lab} = 450$ GeV), E866 ($p_{\rm lab} = 800$ GeV), and HERA-B ($p_{\rm lab} = 920$ GeV). Points and curves of the same color are at the same energy. No IC is shown in (a) while $P^0_{\rm ic\,5} = 0.1\%$, 0.3%, and 1% are in (b)-(d).

$\alpha(x_F)$ for Fixed-Target J/ψ Data

E866 J/ψ x_F and p_T Distributions $(p+p)$

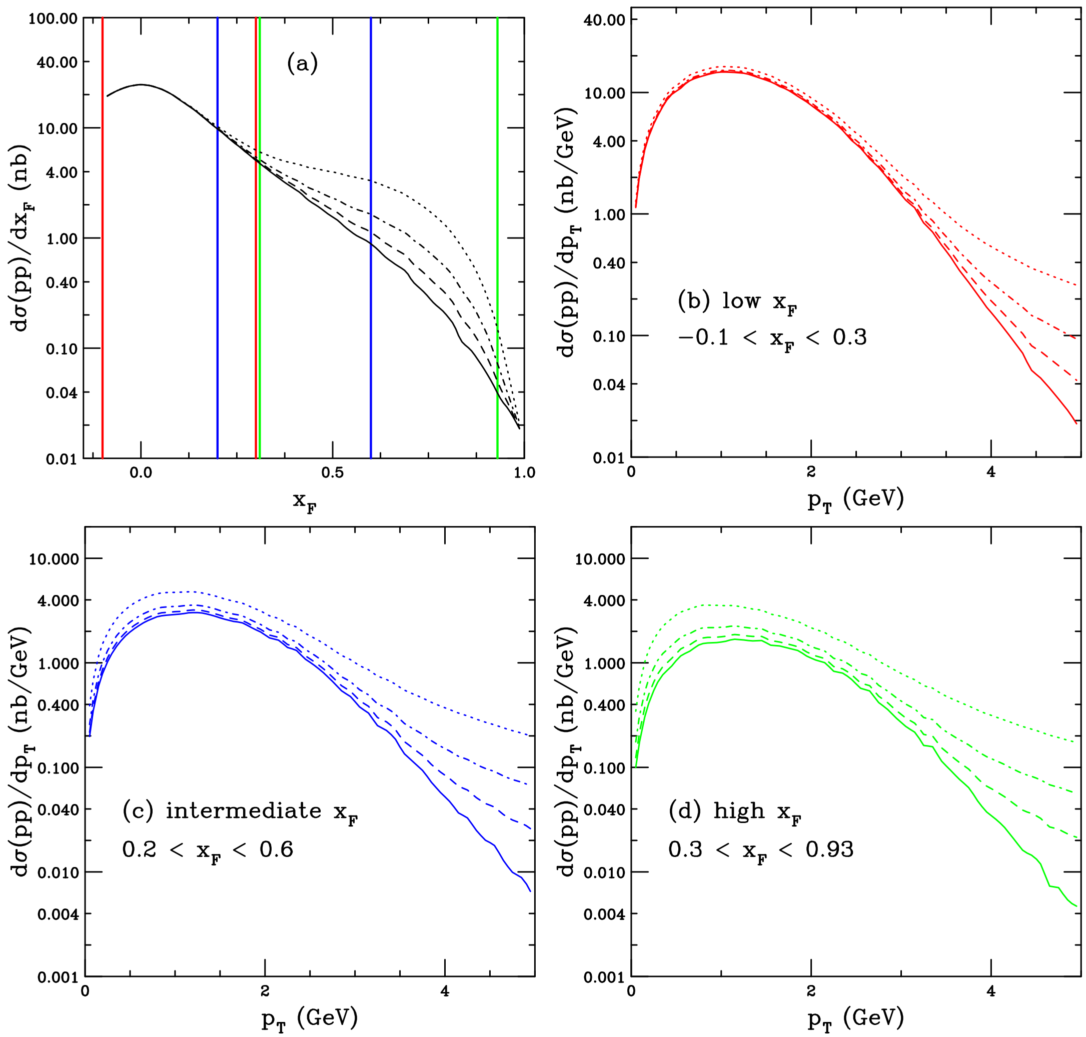

Figure 9: The J/ψ cross sections in $p+p$ collisions at $\sqrt{s} = 38.8$ GeV with and without IC as a function of x_F (a) and p_T at low (b), intermediate (c), and high x_F (d). The solid curves do not include IC while the dashed, dot-dashed and dotted curves use $P^0_{\rm ic\,5} = 0.1\%$, 0.31% and 1% respectively. The colored vertical bars on the x_F distributions show the x_F limits of the p_T distributions in (b)-(d) and matches the color of the curves in (b)-(d). RV, PRC **103**, 035204 (2021).

Comparison with α Extracted from E866 J/ψ $p + A$ Data

E866 obained α as a function of x_F and p_T (in 3 x_F bins) from Be, Fe, and W targets

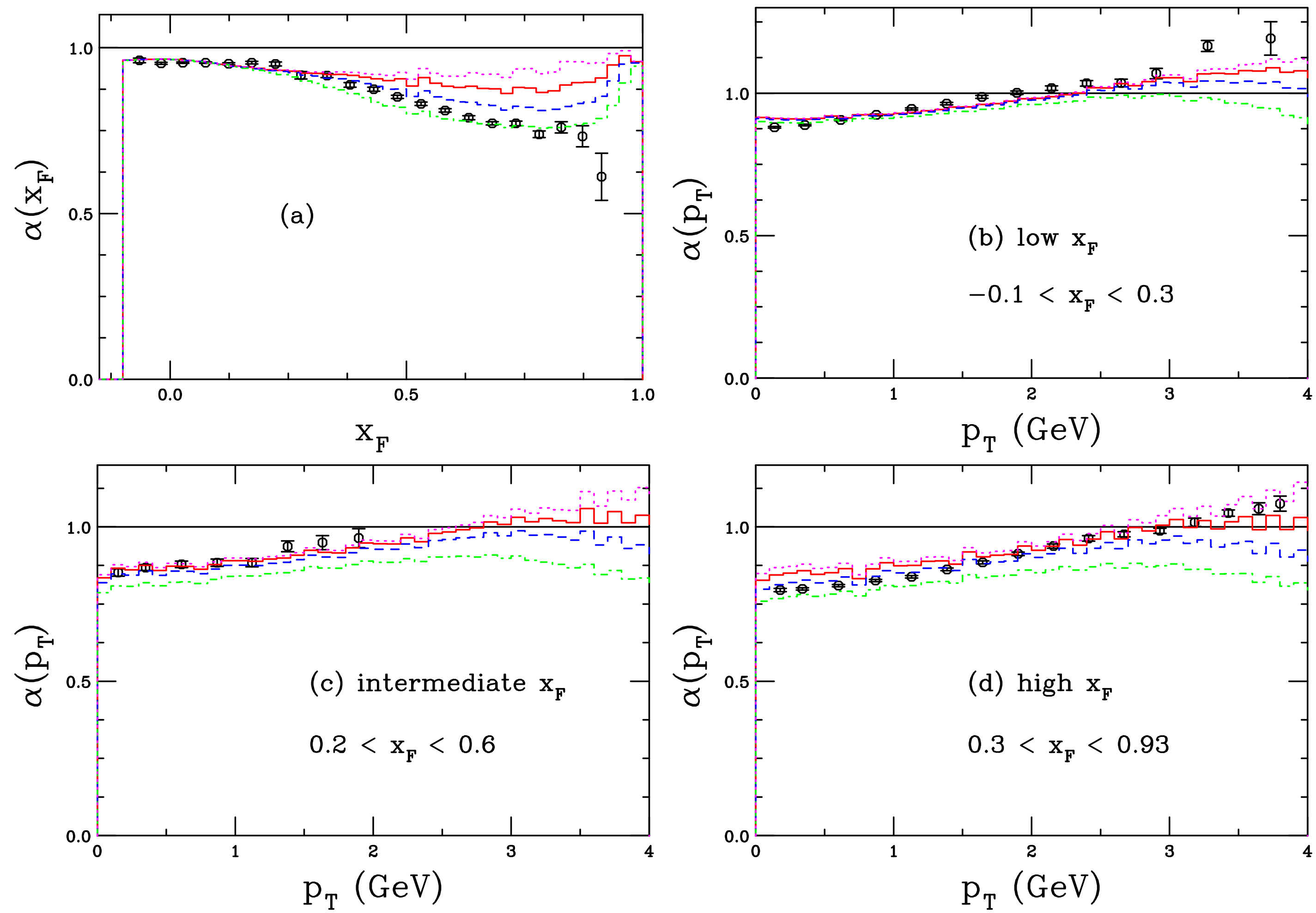

Figure 10: The exponent $\alpha(x_F)$ (a) and $\alpha(p_T)$ for low x_F (b), intermediate x_F (c), and high x_F (d). The dotted magenda curves use $P^0_{\rm ic\,5} = 0$ while the solid red, dashed blue, and dot-dashed green curves show $P^0_{\rm ic\,5} = 0.1\%$, 0.31% and 1% respectively. The E866 data (PRL **84**, 3256 (2000)) are the black points. From: RV, PRC **103**, 035204 (2021).

SMOG J/ψ Results for $\sqrt{s_{NN}} = 69$ GeV $p+\mathrm{Ne}$ Data

Preliminary SMOG J/ψ data shown at QM2022, with a paper in preparation

SMOG has previously published [Phys. Rev. Lett. 122, 132002 (2019)] data for $p+\mathrm{He}$ at $\sqrt{s_{NN}} = 87.7$ GeV and $p+\mathrm{Ar}$ at $sqrts_{NN} = 110.4$ GeV, both for J/ψ and for D mesons

Calculations are in progress to compare with these data, as well as expected data on D & $\overline{D}$ asymmetries which should be non-zero if intrinsic charm is significant: $\overline{D}$ can be produced from a $|uudc\overline{c}\rangle$ state while D cannot – $\overline{D}$ is leading charm while D is nonleading

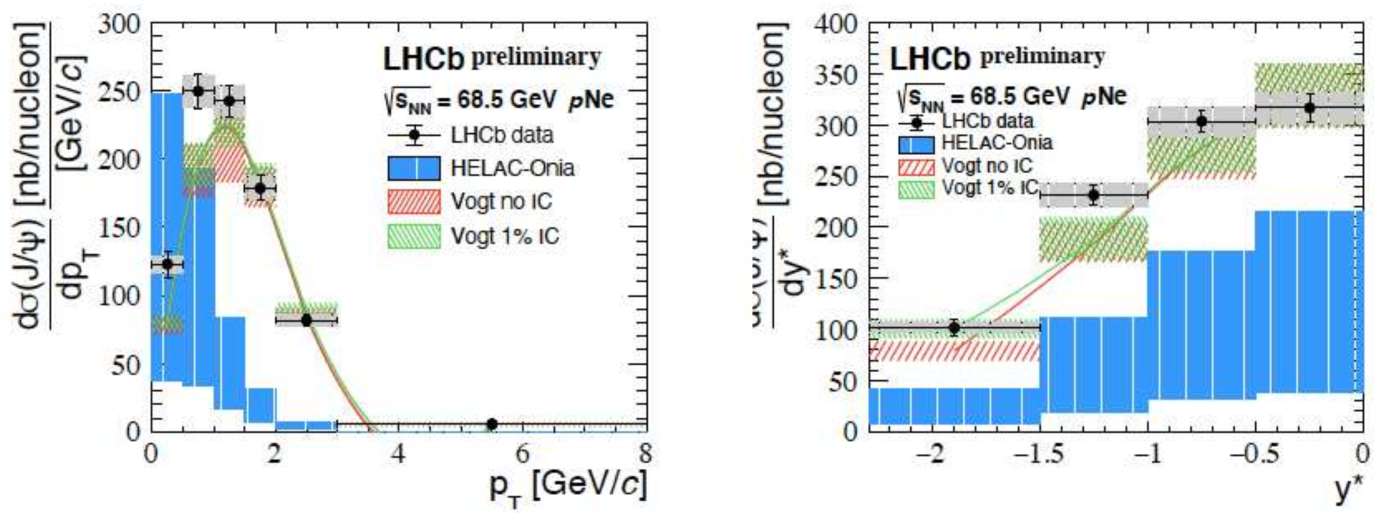

Figure 11: SMOG $p+\mathrm{Ne}$ data at $\sqrt{s_{NN}} = 69$ GeV compared to this model and HELAC-ONIA. The agreement with this model is very good but the data cannot distinguish the presence or absence of intrinsic charm to any significance.

Rapidity and p_T $p + \mathrm{Pb}$ Ratios: No Intrinsic Charm

Upper curves do not include absorption, lower curves employ $\sigma_{\rm abs}$ from 11 mb for $p_{\rm lab} = 40$ GeV to 0 for $\sqrt{s_{NN}} = 5$ TeV

Rapidity distributions do not depend on k_T kick, only absorption, increasing beam energy broadens rapidity distribution, increasing absorption gives lower $R_{p\rm Pb}$

p_T distributions without k_T kick flat, higher incident energy goes further into anti-shadowing region, increasing energy also increases size of k_T kick

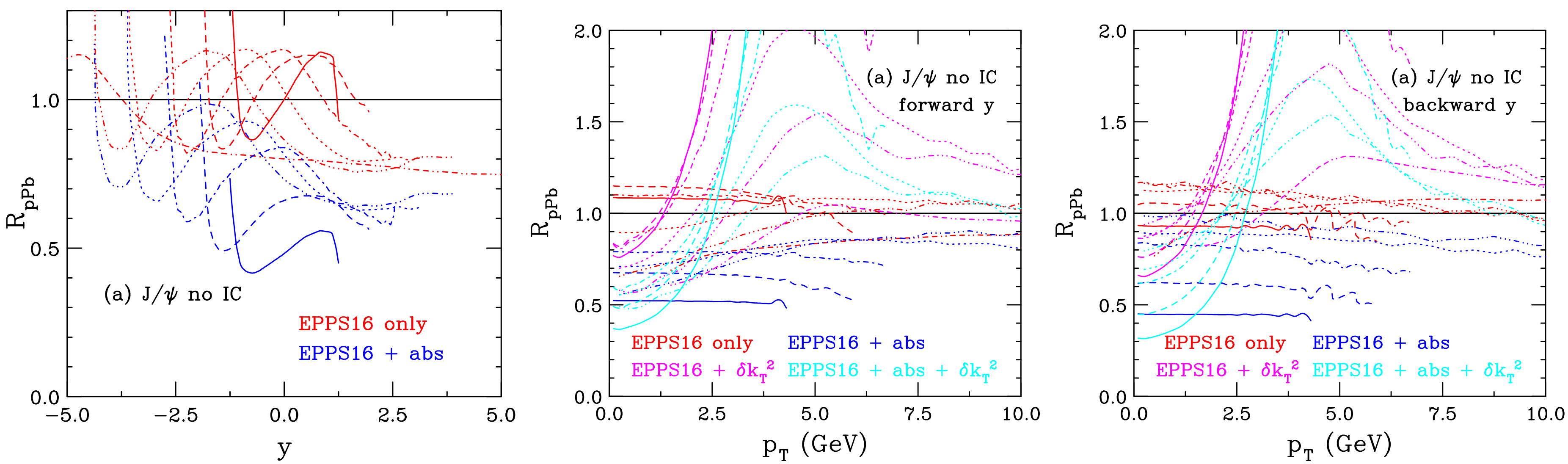

Figure 12: The nuclear modification factors for J/ψ production as a function of y (left) and p_T (right) for pQCD production alone for lead targets relative to proton. The rapidity distributions do not depend on the k_T broadening.

$R_{p\mathrm{Pb}}$ as a function of y and p_T: With 1% Intrinsic Charm

The p_T results are shown for forward rapidity, backward rapidity is similar. The $R_{p\mathrm{Pb}}$ with intrinsic charm has a minimum in A dependence at $A^{\beta-1} = 0.213$, reached at higher p_T for larger $\sqrt{s_{NN}}$.

At low center of mass energies, the IC rapidity distribution is not boosted very much so IC has the biggest effect at low $\sqrt{s}$ but becomes negligible there at higher energies. (Lower IC % gives similar results – same limit – but less suppression.)

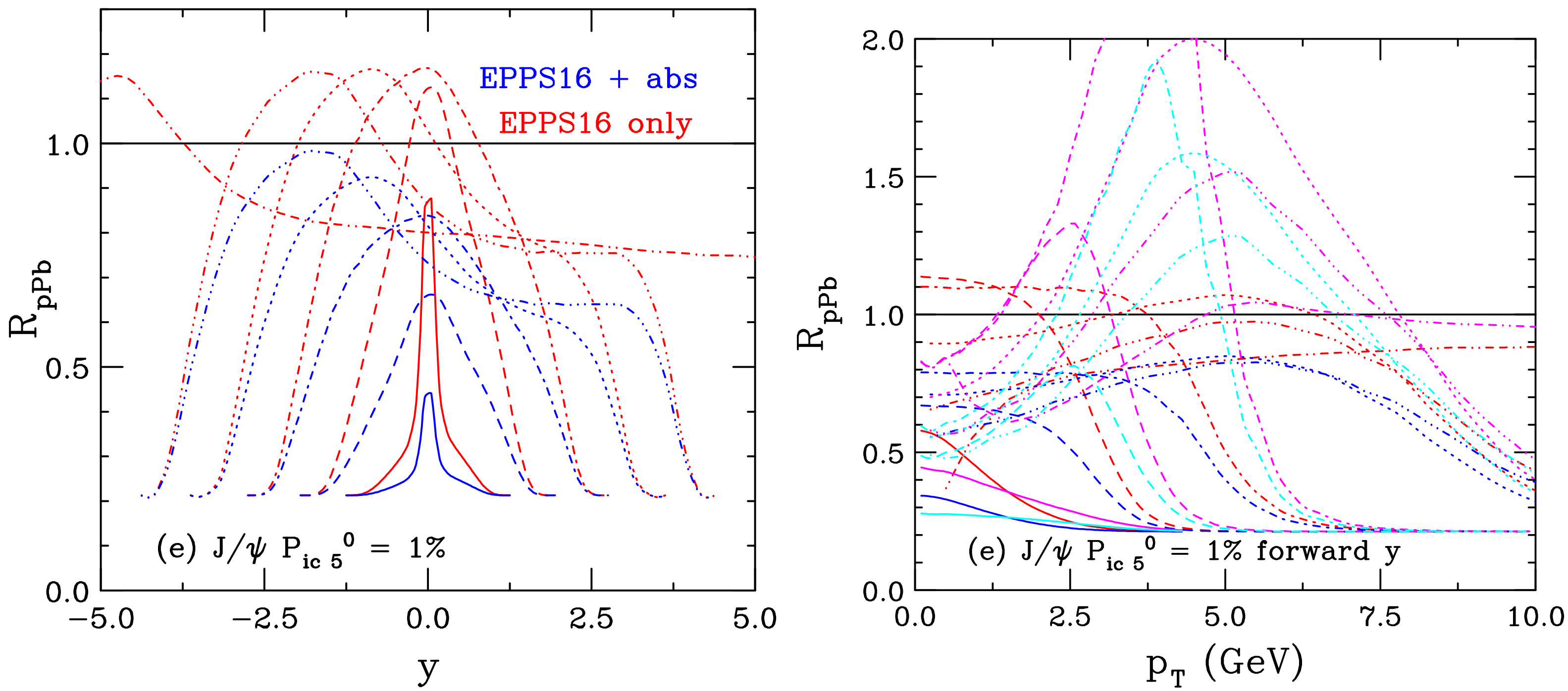

Figure 13: The nuclear modification factors for J/ψ production as a function of p_T for lead targets relative to proton with $P^0_{\mathrm{ic}\,5} = 1\%$ as a function of rapidity (left) and p_T (right). The red curves include the EPPS16 modifications of the parton densities only while the blue curves also include nuclear absorption of the J/ψ. The magenta curves include the EPPS16 modifications as well as k_T broadening while the cyan curves include EPPS16, nuclear absorption for the J/ψ, and k_T broadening. The line types denote different energies: $p_{\mathrm{lab}} = 40$ GeV (solid), 158 GeV (dashes), 800 GeV (dot-dashed), $\sqrt{s_{NN}} = 87.7$ GeV (dotted), 200 GeV (dot-dot-dot-dashed) and 5 TeV (dot-dot-dash-dashed). Note that the rapidity range is $0 < y < 1$ for all energies except the two highest where the rapidity range is $1.1 < y < 2.2$ for 200 GeV and $2.5 < y < 5$ for 5 TeV.

Summary

Cold nuclear matter effects include absorption, nPDFs, transverse momentum broadening, and intrinsic charm

Combined model agrees well with fixed-target data; intrinsic charm too far boosted in rapidity to play a role at collider energies and even in most fixed target experiments close to midrapidity

The low center of mass energies of NA60+ could provide stringent constraints on the energy dependence of intrinsic charm in the hadron wavefunction

The same formalism is being applied to J/ψ and D^0 production with the fixed-target SMOG device for LHCb, as shown for the $p + \mathrm{Ne}$ data, stay tuned